Computational Condensed Matter 33 (2022) e00745

Contents lists available at ScienceDirect

Computational Condensed Matter

journal homepage: www.elsevier.com/locate/cocom

Modulation of the optoelectronic properties of $CdSe_2$

B. Thapa [a,b], P.K. Patra [a], Abeer E. Aly [c,d], M. Das [b], A. Shankar [b,*]

[a] Department of Physics, North-Eastern Hill University, Shillong, 793022, India
[b] Condensed Matter Theory Research Lab, Department of Physics, Kurseong College, Darjeeling, 734203, India
[c] Basic Science Department, Al Salam Higher Institution for Engineering and Technology, Cairo, Egypt
[d] Physics Department, Higher Institution for Engineering, El Shorouk Academy, Cairo, Egypt

ARTICLE INFO

Keywords:
Transition metal dichalcogenides
Absorption coefficient
Dielectric
GGA
mBJ

ABSTRACT

Based on density functional theory, the first-principles calculations are carried out to study the optoelectronic properties of $CdSe_2$ under hydrostatic pressure. The GGA calculation predicts the energy band gap of 0.546 eV that has been enhanced to 1.473 eV due to the inclusion of mBJ functional in the study. The current theoretical calculations present semiconductor to metal transitions at 5.1 GPa for GGA and 8.1 GPa for mBJ functional. The application of pressure (10 GPa and −8 GPa) has also successfully reproduced better optical responses like refractive index, reflectivity, and optical conductivity with an enhanced absorption coefficient of 4.867×10^5 cm^{-1}. Their optical and electronic properties are of particular interest and suitable for applications in optoelectronics as photovoltaic devices, light emitters, and detectors.

1. Introduction

Transition metal dichalcogenides (TMDCs) have been continuously studied for their photocatalytic [1] and photovoltaic [2] applications, owing to their exceptional properties like strong absorption in the solar spectrum region. They have also been proposed for logic circuits [3] and memory devices [4]. Cadmium dichalcogenides (CdX_2; X = S, Se, Te), stable in their pyrite structure [5–7] belonging to this family have gained popularity among researchers after the successful synthesis of CdS_2 and $CdSe_2$ at high pressures (6.5–8.9 GPa) in 1968 [6]. Later on, Rouset et al. [8] also fabricated $CdTe_2$ using a cost-effective wet electrodeposition technique in 2008. $CdTe_2$ and $CdSe_2$ have higher absorption coefficients [5] and optical response may be further enhanced to make them an effective candidate for photovoltaic applications. In the literature, it has been observed that in the course of tuning the electronic and optical properties of a material to make them an efficient candidate for technological and energy devices, the effect of hydrostatic pressure has become one of the efficient tools [9]. Furthermore, exploiting the effect of pressure on the behavior of the material is also interesting as useful information and specific characteristics can be gained during the study [9,10]. In the literature, several reports can be found on the pressure-induced technique on TMDCs. Javed et al. [11] have shown a significant decrease in the lattice constants with the hydrostatic pressure, which further induces the electronic structure. In some of the semiconductors like MoS_2, the application of pressure above 35 GPa makes it semi-metallic [12]. Similarly, the electronic bandgap of marcasite $FeSe_2$ increases with pressure, making it suitable for photovoltaic applications, whereas, for the pyrite phase, it transforms from semiconductor to metal at 65 GPa [13]. Liu et al. [14] have demonstrated semiconductors to the semimetal phase transition of WSe_2 at a pressure of 38.1 GPa from their electrical resistivity spectra and the first-principles calculations. Likewise, Deng et al. [15] also observed enhanced reflectivity, absorption coefficients, and reflectivity of PdS_2 with pressure.

In the literature, there exist several studies reporting the semiconducting properties of $CdSe_2$ [6,7] with optical response in the suitable frequency range effective for optoelectronic devices. Similarly, external hydrostatic pressure has become a successful tool to modulate material's behaviour which further motivated us to explore the effect of pressure on the optoelectronic properties of $CdSe_2$. Hence, in the present manuscript, we have studied the electronic properties of the semiconducting pyrite type $CdSe_2$ using the first-principles calculation by including efficient mBJ functional. The effect of pressure in the range of −10 to 10 GPa is also verified in the electronic properties of the material. The response of the optical behaviour of this binary alloy is also investigated with a motive to improve the optical absorption of this semiconductor making it a suitable candidate for optical applications.

* Corresponding author.
E-mail address: amitshan2009@gmail.com (A. Shankar).

https://doi.org/10.1016/j.cocom.2022.e00745
Received 13 April 2022; Received in revised form 7 September 2022; Accepted 8 September 2022
Available online 13 September 2022

2. Computational details

All the total energy calculations and electronic and optical properties of $CdSe_2$ are performed using the full-potential linear augmented plane wave (FP-LAPW) method as implemented in the wien2k [16]. It is based on the density functional theory (DFT), which is one of the most efficient simulation methods for the calculation of ground-state state properties of the materials [17]. The generalized gradient approximation (GGA), as flavoured by Perdew, Burke and Ernzerhof (PBE) [18], is employed for electron exchange-correlation energy. The calculations are performed using $R_{MT} \times k_{max} = 7$, which determines the matrix size to achieve energy eigenvalues convergence, where R_{MT} is the smallest muffin-tin radius and max is the maximum modulus for the reciprocal lattice vectors. The values of muffin-tin radii for Cd and Se are taken as 2.5 a.u and 2.27 a.u, respectively. The self-consistent potentials are calculated on a $10 \times 10 \times 10$ k-mesh in the Brillouin zone and the self-consistency convergence criterion is set to 10^{-4} Ry. In the interstitial region, the charge density is expanded as a Fourier series with wave vectors $G_{max} = 12$ a.u.$^{-1}$. The electronic and optical properties of this compound under pressure are studied in the range of −10 to 10 GPa.

3. Results and discussion

3.1. Structural properties

The pyrite $CdSe_2$ crystallizes in a cubic structure (space group *Pa*-3) with Wyckoff position 4a (0, 0, 0) and 8c (*u, u, u*) for Cd and Se, respectively (Fig. 1), where *u* is the internal parameter. In this work, our lattice constant and internal parameter (*u*) is 6.745 Å and 0.397, respectively, where the lattice constant is higher than the experimental value (6.615 Å) as expected from the GGA functional [6] and is in good accordance with the theoretical report (6.743 Å) [5]. The thermodynamic stability of $CdSe_2$ is verified by estimating the formation energy (ΔE_F) [19,20] as given by the equation,

$$\Delta E_F = [E_{Tot} - (xE_{Cd} + yE_{Se})] / (x+y) \quad (1)$$

where, E_{Tot} is the total energy of the compound, E_{Cd} and E_{Se} are the equilibrium energy of the Cd and Se atoms, which are found to be −11192.070 Ry and −4860.240 Ry, respectively. Here, *x* and *y* denote the number of Cd and Se atoms, respectively. The negative formation energy per formula unit per atom (−0.1587 Ry) indicates their thermodynamic stability [21].

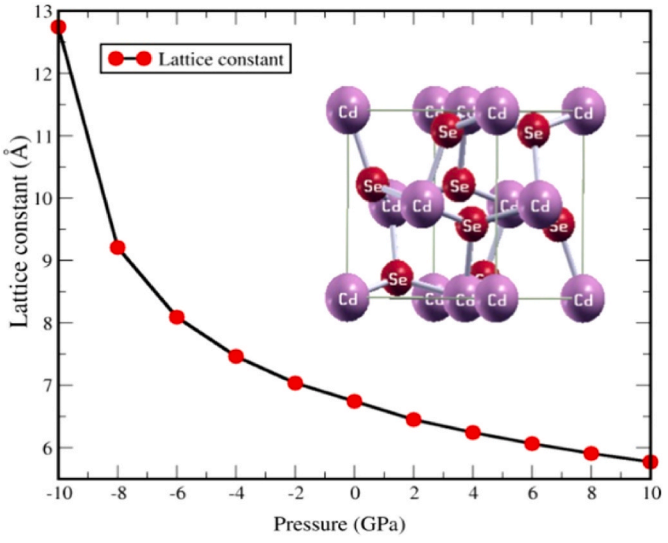

Fig. 1. Variation of lattice constant with pressure and unit cell structure of $CdSe_2$ (figure inset).

The material was applied with external pressure in the range of −10 to 10 GPa, where we find that the lattice constant of $CdSe_2$ decreases continuously, as shown in Fig. 1 following the Murnaghan equation of state [22] as given by Eq. (2). Here, one can note that with the increase of pressure, the distance between the atoms decreases due to compression and hence, their repulsive interaction is strengthened, which leads to a decrease in the lattice constant and the cell volume.

$$P(V) = \frac{B_o}{B_o'}\left[\left(\frac{V_o}{V}\right)^{B_o'} - 1\right] \quad (2)$$

where V_o is the solid's equilibrium volume, B_o represents the bulk modulus and B_O' is the first pressure derivative of the bulk modulus. The stability of the structure so formed after the use of external pressure was also verified from their formation energy. We found that at 10 and -10 GPa the formation energy was found to be −83650.75 Ry and −83650.17 Ry, respectively. The negative formation energy of this compound at −10 and 10 GPa validates the thermodynamic stability of this compound.

3.2. Electronic properties

To understand the electronic nature of $CdSe_2$, their energy band structure along the high symmetry directions of the Brillouin zone (BZ) is calculated as shown in Fig. 2. The figure reflects a distinct semiconducting nature with an indirect band gap of 0.546 eV with the valence band maximum at the Γ point and the conduction band minimum between *R* and Γ point. Olsson et al. [5] also reported consistent values of 0.575 eV, 0.508 eV, and 1.439 eV using the PBE, LDA, and GW functional, respectively. Whereas, Jia et al. [23] have reported the energy band gap of 1.472 eV using the Heyd–Scuseria–Ernzerhof (HSE06) method, whereas 0.588 eV using GGA functional. No experimental band gap of $CdSe_2$ has been reported so far and since GGA underestimates the band gap, we have also incorporated the computationally cheap but highly accurate modified Becke-Johnson potential (mBJ) to yield the energy band structure [24,25]. The overall band profile of mBJ estimated bands is similar to GGA but the energy band gap of $CdSe_2$ increases to 1.473 eV, comparable to reports of Jia et al. [23] and Olsson et al. [5]. The infusion of mBJ shifts the conduction bands to the higher energy level leading to an increase in the energy band gap. This is because mBJ imposes semi-localization on the valence electrons of the material. This as a result restricts the occupation number of electrons in the valence orbital. So, an electron that is considered a valence under the GGA scheme will be neglected under semi localization scheme of mBJ. Therefore, the overall energy of atom decreases thereby shifting the conduction band to the higher energy level or the valence bands to the lower energy level.

The dispersion of the conduction band (CB) of $CdSe_2$ is fairly flat around Γ and, in combination with the heavy holes (Γ-*X*) valence band, may induce significant absorption coefficients. Fig. 2b shows the total and partial density of states of $CdSe_2$, where the vicinity of the Fermi energy region (E_F) mainly consists of contributions from the Cd-*d* and Se-*p* states. The sharp peak contributed by the Se-*p* states at 1.47 eV can be seen as flat bands in the band structure. At a higher energy range (4–6 eV), we find states arising from the Cd-*p* states. In contrast, at the energy range of 2–3 eV of the conduction bands, the states are mainly composed of Cd-*s* states hybridized with Se-*p* states. At the lower energy range (<-4eV) of valence bands, the bands constitute an equal mixture of Cd-*s* and Se-*p* states. The low-lying Cd-4*d* states in this compound influence the DFT predicted band gap [26,27] through a *p*-*d* coupling [28].

We have also studied the application of pressure on the sample material, where the pressure impacts the energy band gap of the material. Fig. 3 displays the variation of the energy band gap with pressure. The material sustains its semiconducting behaviour up to a pressure of 5 GPa and at 5.1 GPa, $CdSe_2$ transforms into a metallic phase. At 4 GPa,

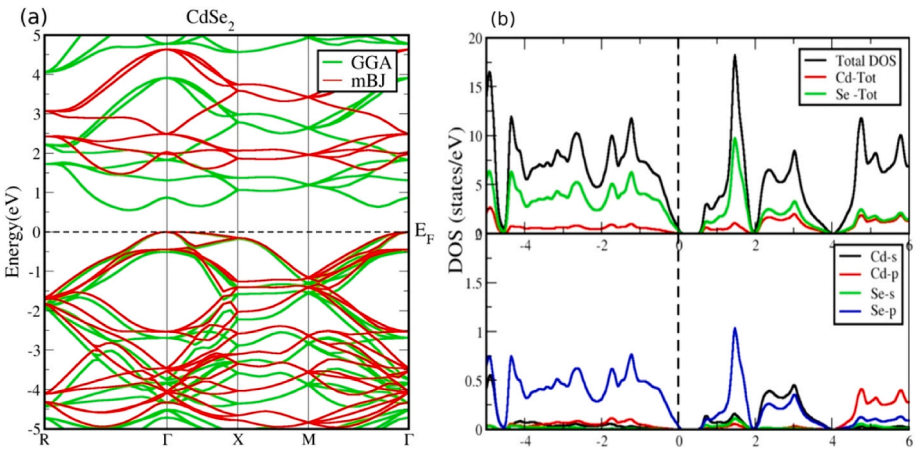

Fig. 2. (a) Energy band structure and (b) density of states of $CdSe_2$.

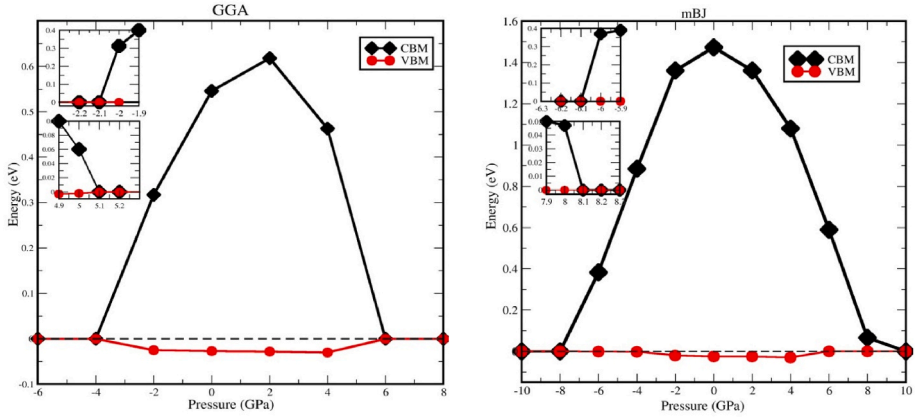

Fig. 3. Valence band maxima and conduction band minima under pressure.

the valence band maximum (VBM) is still positioned at Γ point, but the conduction band minimum (CBM) position shifts from between R - Γ to Γ point, making it a direct band gap semiconductor with an energy band gap of 0.478 eV. The material sustains its semiconducting behaviour at −2 GPa and with a further decrease in pressure that is at −2.1 GPa, the material starts to behave like a metal. The applied pressure causes the CBM to rise towards the E_F; hence the energy band gap decreases monotonically with pressure till a semiconductor-metal transition occurs at 5.1 GPa. With further increase in the pressure, the conduction bands shift towards the valence bands leading to the overlap of two bands. Here, applying pressure compresses the crystal's size and increases the existing interlayer interaction, leading to the metallic nature of the system. Also, the valence band around the E_F is mainly contributed by the *p*-orbital of the Se, while the d-orbital of the Cd mainly contributes to the conduction band near the E_F. The energy splitting between the Se-*p* and Cd-*d* decreases with increasing strain, leading to semiconductor to metal transition at 6 GPa. Many previous experimental and theoretical reports [29,30] of the analogous compounds have reported similar variations of the energy band gap with pressure indicating a higher electrical conductivity at high pressures. With the infusion of mBJ, the semiconductor-metal transition occurs at 8.1 GPa, so at 6 GPa, the materials still behave as a semiconductor when treated with the mBJ functional. Hence, the compound sustains its semiconducting nature in −2 to 5 GPa when treated with GGA and in −6 to 8 GPa when treated with mBJ functional.

3.3. Optical properties

The electronic band structure of $CdSe_2$ directly influences their optical properties, which is an essential parameter for device applications. Since the energy band gap value found by mBJ functional was better and closer to other theoretical reports, we have retained the results obtained by mBJ functional to further calculate the optical properties of $CdSe_2$. The optical properties were deliberated based on the obtained results of dielectric functions ε(ω), defined as $\varepsilon(\omega) = \varepsilon_1(\omega)+i\varepsilon_2(\omega)$, where $\varepsilon_1(\omega)$ is the real part and $\varepsilon_2(\omega)$ is the imaginary part of the dielectric constant; $\varepsilon_2(\omega)$ given as [31].

$$\varepsilon_2(\omega) = \frac{Ve^2}{2\hbar\pi m^2\omega^2} x \int d^3k \sum_{nn'} |kn|p|kn'|^2 f(kn)[1-f(kn')]\partial(E_{kn} - E_{kn'} - \hbar\omega) \tag{3}$$

The integral is taken over the first Brillouin zone, where p is the momentum matrix element between n and n' states, $<kn|$ is the crystal wave function with an eigen value E(*kn*) and f(*kn*) is the Fermi distribution function. The real part of the dielectric function can be determined using the Kramers-Kronig relations,

$$\varepsilon_1(\omega) = 1 + \frac{2}{\pi}\int_0^\infty \frac{\varepsilon_2(\omega')\omega' d\omega'}{\omega'^2 - \omega^2} \tag{4}$$

The real part of dielectric function $\varepsilon_1(\omega, P)$ at different hydrostatic pressures is presented in Fig. 4. The real part increases gradually with energy and attains maxima followed by a valley below zero amplitude which is due to the damping of the electromagnetic wave. The zero

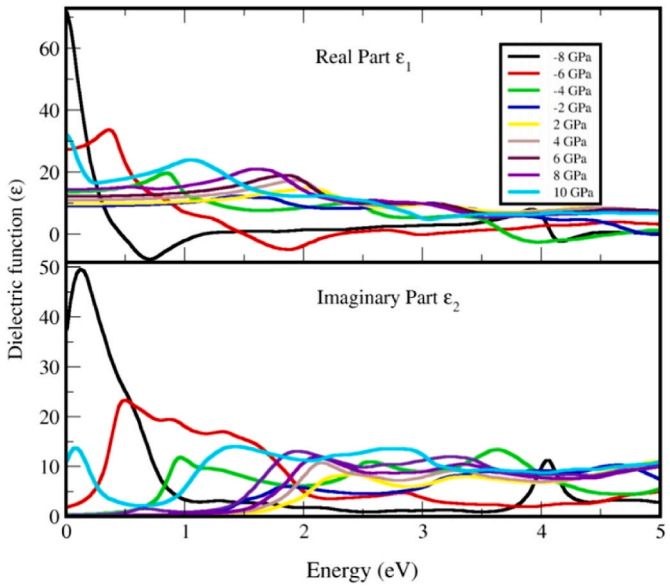

Fig. 4. Real and imaginary parts of the dielectric function for different pressure.

values also indicate the possibility of longitudinally polarized waves. The peaks of the real and imaginary parts of the dielectric functions fall at the same energy range of 0–2 eV, which implies the low oscillator strength of interband transitions. Here, the effect of hydrostatic pressure on the evolution of static dielectric function $\varepsilon_1(0, P)$ in the limit of $\omega \to 0$ is obtained and the values are intimidated in Table 1. The static dielectric function changes with the application of pressure, where the maximum static dielectric function is found at −8 GPa, which is 71.4, and from there, the value gradually decreases under compression with their value of 27.4, 13.7, and 9.04, for −6, −4 and −2 GPa pressure, respectively. Thereafter, the further application of pressure increases the static dielectric constant. These values give the threshold for direct optical transitions between the valence band maximum and the conduction band minimum. Beyond these points, the curve increases rapidly because the number of points contributing towards $\varepsilon_2(\omega)$ increases. In addition, we can find several peaks for the imaginary part, which reflects transitions between different orbitals. For the largest strain, the amplitudes of both the real and imaginary parts are much higher, demonstrating that many inter-band transitions occur at this energy, corresponding to the concentrated bands near the E_F. One of the remarkable features of $\varepsilon_2(\omega, P)$ is that the amplitude of $\varepsilon_2(\omega, P)$ moves to the lower photon energy with increasing hydrostatic pressure, as shown in Fig. 4, as the energy band gap of $CdSe_2$ decreases when hydrostatic pressure increases.

The refractive index (μ), defined as the ratio of the speed of light in a vacuum to the speed of light in a medium, measures the transparency of materials and hence plays a vital role in designing optical devices. In terms of the real and imaginary parts, we can derive the refractive index and extinction coefficient given by

$$\mu = \sqrt{\frac{\sqrt{\varepsilon_1^2 + \varepsilon_2^2} + \varepsilon_1}{2}} \tag{5}$$

$$k = \sqrt{\frac{\sqrt{\varepsilon_1^2 + \varepsilon_2^2} - \varepsilon_1}{2}} \tag{6}$$

The static refraction coefficient is highest for −8 GPa and decreases further with the removal of pressure. Thereafter, with the application of pressure, the value of the static refraction coefficient tends to increase. The application of pressure of less than −2 GPa and greater than 5 GPa, leads to a transition of semiconducting to a metallic state; hence the refractive index is higher at this range of pressure due to the interband transitions of electrons. The curve of refractive index as a function of energy increase to the maximum value of 8.7, 5.9, 4.5, 3.5, 3.9, 4.2, 4.4, 4.6, and 5.7 for the pressure of −8, −6, −4, −2, 2, 4, 6, 8 and 10 GPa, respectively, in the energy range of 0–2 eV (Fig. 5). After attaining a maximum value, the refractive index gradually decreases in a higher energy range and becomes almost equal to unity, and the materials behave as a vacuum. Olsson et al. [5] have reported the static refractive index of $CdSe_2$, which is following the present report (Table 1).

The optical absorption coefficient can be expressed as,

$$\alpha = 2\frac{\omega k}{c} \tag{7}$$

where ω and c are the angular frequency and speed of light, respectively. However, the change in the absorption coefficient is in contrast to the refractive index, where the graph of absorption coefficient increases gradually in the higher energy range, as shown in Fig. 6. We also find maximum absorption for minimal dispersion of $\varepsilon_1(\omega)$, which corresponds to maximum conduction. In the visible energy range, the absorption coefficient is highest for −4 GPa which is found to be $0.4867 \times 10^6\ cm^{-1}$. For the pressure of 8 GPa, the absorption coefficient is found to be $0.485099 \times 10^6\ cm^{-1}$ in the visible energy range. With the increase in pressure, the peak value of the absorption coefficient of $CdSe_2$ also increases.

Table 1
The static dielectric constant, static refraction coefficient, and static reflection coefficient at different pressures.

Pressure (GPa)	Static Dielectric Constant	Static Refraction Coefficient	Static Reflection Coefficient
−8	71.4	8.7.	0.68
−6	27.4	5.2	0.46
−4	13.7	3.7	0.33
−2	9.04	3	0.25
2	9.76	3.1	0.26
4	11.0	3.3	0.28
6	12.2	3.5	0.31
8	14.4	3.8	0.34
10	32.1	5.7	0.51

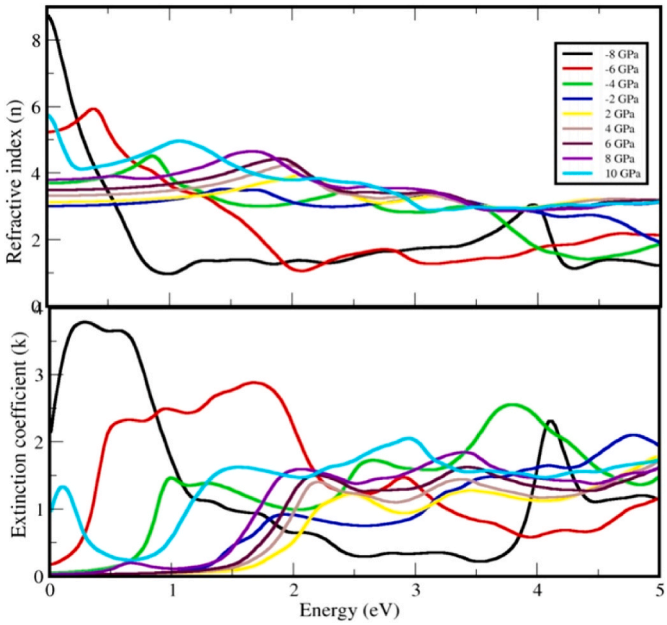

Fig. 5. Refractive index and extinction coefficient of $CdSe_2$ for different pressure.

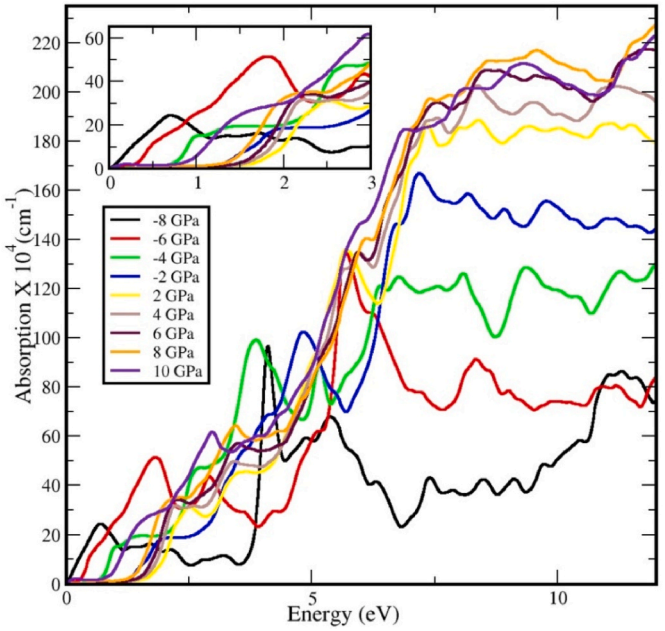

Fig. 6. Absorption spectra of $CdSe_2$ under different pressure.

The reflectivity (R) describes how much light is reflected from the material about an amount of light incident on the material and can be written as,

$$R = \frac{(1-n)^2 + k^2}{(1+n)^2 - k^2} \tag{8}$$

Reflectivity spectra of $CdSe_2$ versus photon energy under selective hydrostatic pressure are drawn in Fig. 7. The static value of reflection continuously increases in the higher energy range for all the pressure values. It is also worth noting that the maximum reflection can be seen where the value of $\varepsilon_1(\omega)$ is negative. The minimal value of the reflection coefficient depicts less reflection of incident rays making the material transparent in a particular energy range. The change in pressure from −8 to −6 GPa leads to a value of reflection coefficient, which contradicts each other, where at 4 eV, the reflection is maximum for −4 GPa, whereas for −6 GPa, the reflection is minimum.

However, with the application of pressure, we notice an insignificant change in the reflectivity spectra of the material. Another important aspect is that increasing hydrostatic pressure also drives the peaks in the R(ω) shift towards lower photon energy levels. For the pressure of −8 GPa, the reflectance spectra in the energy range of 2 eV–4 eV are below 20%, making the material opaque in that particular range. This result is further supported by the absorption curve (Fig. 6), where we find that the absorption coefficient is significant for this specific range as more absorption means less reflection. The increase of reflectivity under positive pressure suggests the starting of the pressure-induced metallization in $CdSe_2$.

4. Conclusion

In the present study, the electronic and optical properties of semiconducting $CdSe_2$ under pressure have been presented. We find that the semiconductor $CdSe_2$ transforms into metal at a pressure of 8.1 GPa. The critical point of the frequency-dependent complex dielectric function was investigated to analyze the optical transitions. The enhanced optical response of material like reflectivity, conductivity, absorption, and refraction spectra has been studied under pressure. Till now no such experimental and theoretical reports for the variation of optical properties under pressure for the sample are available to the best of our knowledge. The present report also shows that we can tune the properties of $CdSe_2$ with the application pressure without the aid of any dopant which is commercially cheap and also eliminates the complications of finding a suitable dopant and their perfect compositions.

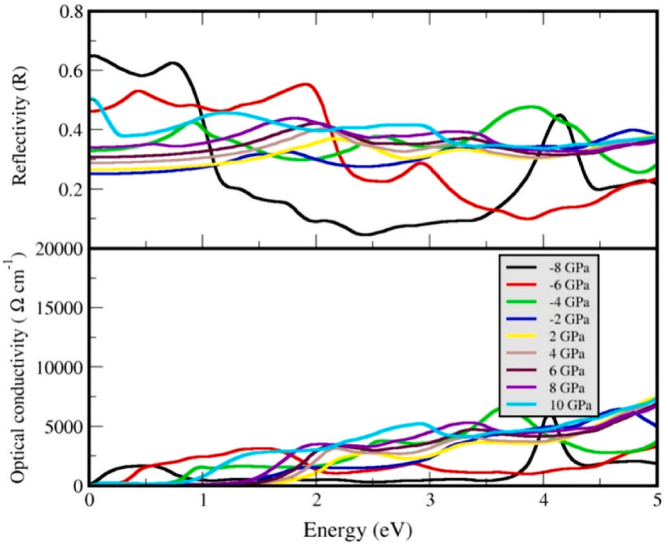

Fig. 7. Reflectivity and optical conductivity of $CdSe_2$ for different pressure.

Author contributions

All the authors contributed equally to bringing the manuscript into its present shape.

Declaration of competing interest

The authors declare that they have no known competing financial interests or personal relationships that could have appeared to influence the work reported in this paper.

Data availability

Data will be made available on request.

Acknowledgments

A.S. acknowledges DST-SERB, India, for research funding (EEQ/2017/000319).

References

[1] W.K. Ho, J.C. Yu, J. Lin, J.G. Yu, P.S. Li, Langmuir 20 (2004) 5869.
[2] Pang Yaokun, Fei Xue, Longfei Wang, Jian Chen, Jianjun Luo, Tao Jiang, Chi Zhang, Zhong Lin Wang, Adv. Sci. 6 (2016), 1500419.
[3] B. Radisavljevic, M.B. Whitwick, A. Kis, ACS Nano 5 (2011) 9934.
[4] S. Bertolazzi, D. Krasnozhon, A. Kis, ACS Nano 7 (2013) 3246.
[5] P. Olsson, J. Vidal, D. Lincot, J. Phys. Condens. Matter 23 (2011), 405801.
[6] T.A. Bither, R.J. Bouchard, W.H. Cloud, P.C. Donohue, W.J. Siemons, Inorg. Chem. 7 (1968) 2208.
[7] A.A. Musari, D.P. Joubert, G.A. Adebayo, Phys. B Condens. Matter 552 (2019) 159–164.
[8] J. Rousset, P. Olsson, B. Mc Candless, D. Lincot, Chem. Mater. 20 (2008) 6555.
[9] Dinesh Varshney, Geetanjali Dagaonkar, Meenu Varshney, Mater. Res. Bull. 45 (2010) 926.
[10] Lu-Gang Cai, Fa-Min Liu, Dian Zhang, Wen-Wu Zhong, Physica B 408 (2013) 78.
[11] Y. Javed, M.A. Rafiq, Nisar Ahmed, Royal Soc. Chem. 7 (2017), 38843.
[12] H. Peelaers, C.G. Van de Walle, J. Phys. Chem. C 22 (2014), 12076.
[13] Mingsheng Yi, Jintao Wu, Xiaojun Zheng, Ming Xing, Eur. Phys. J. B 93 (2020) 1–9.
[14] Bao Liu, Yonghao Han, Chunxiao Gao, J. Phys. Chem. C 114 (2010), 14254.
[15] Shuo Deng, Menglun Tao, Jie Mei, Min Li, Yan Zhang, Lijie Li, IEEE Trans. Nanotechnol. 18 (2019).
[16] P. Blaha, K. Schwarz, G.K.H. Madsen, D. Kvasnicka, J. Luitz, R. Laskowski, F. Tran, L.D. Marks, in: K. Schwarz (Ed.), WIEN2k 18.2, revised edition, Techn. Universität, Wien, Austria, 2017, ISBN 3-9501031-1-2.

[17] K.M. Wong, S.M. Alay-e-Abbas, Y. Fang, A. Shaukat, Y. Lei, J. Appl. Phys. 114 (2013), 034901.
[18] J.P. Perdew, K. Burke, Y. Wang, Generalized gradient approximation for the exchange-correlation hole of a many-electron system, Phys. Rev. B 54 (1996), 16533.
[19] X. Wang, X. Dai, L. Wang, X. Liu, W. Wang, G. Wu, C. Tang, G. Liu, J. Magn. Magn Mater. 378 (2015) 16–23.
[20] Z.H. Zeng, F. Calle-Vallejo, M.B. Mogensen, J. Rossmeisl, Phys. Chem. 15 (2013) 7526–7533.
[21] N.A. Zarkevich, T.L. Tan, D.D. Johnson, Phys. Rev. B 75 (2007), 104203.
[22] F. Murnaghan, Proc. Natl. Acad. Sci. USA 30 (1944) 244.
[23] T. Jia, J. Carrete, Y. Zhang, G.K. Madsen, arXiv Preprint arXiv:2005.05916, 2020.
[24] F. Tran, P. Blaha, Phys. Rev. Lett. 102 (2009), 226401.
[25] Wanxiang Feng, Di Xiao, Ying Zhang, Yugui Yao, Phys. Rev. B 82 (2010), 235121.
[26] O. Zhakarov, A. Rubio, X. Blase, M.L. Cohen, S.G. Louie, Phys. Rev. B 50 (1994), 10780.
[27] W. Luo, S. Ismail-Beigi, M.L. Cohen, S.G. Louie, Phys. Rev. B 66 (2002), 195215.
[28] S.H. Wei, A. Zunger, Phys. Rev. B 37 (1988) 8958.
[29] Nirup Bandaru, Ravhi S. Kumar, Daniel Sneed, Tschauner Oliver, Jason Baker, Daniel Antonio, Sheng-Nian Luo, Thomas Hartmann, Yusheng Zhao, Rama Venkat, J. Phys. Chem. C 118 (2014) 3230–3235.
[30] Zhen-Hua Chi, Xiao-Miao Zhao, Haidong Zhang, Alexander F. Goncharov, Sergey S. Lobanov, Tomoko Kagayama, Masafumi Sakata, Xiao-Jia Chen, Phys. Rev. Lett. 113 (2014), 036802.
[31] M. Gajdoo, K. Hummer, G. Kresse, Linear optical properties in the projector augmented wave methodology, Phys. Rev. B 73 (2006), 045112.